J. Phys. B: At. Mol. Phys. **20** (1987) 3217-3236. Printed in the UK

Low-energy electron impact spectroscopy of OCS and CS_2

W Sohn, K-H Kochem, K M Scheuerlein, K Jung and H Ehrhardt
Fachbereich Physik, Universität Kaiserslautern, D-6750 Kaiserslautern, West Germany

Received 29 September 1986, in final form 12 December 1986

Abstract. Energy and angular dependences of differential cross sections for elastic scattering and vibrational excitation of the fundamental vibrations and some strongly excited overtones for OCS and CS_2 are presented. The impact energy ranges from 0.3 to 5 eV and scattering angles are measured between 12.5 and 138°. Integral elastic, vibrationally inelastic and total cross sections are tabulated. The total cross sections are compared with theoretical results of Lynch *et al.* With few exceptions good agreement is found. The differential cross sections for elastic and inelastic scattering are compared with first Born approximations for dipole, quadrupole and polarisation potential interactions. A body-frame phase-shift analysis has been applied to the experimental data in the energy range below 1.2 eV.

1. Introduction

The molecules CO_2, OCS and CS_2 represent a series of closely related triatomic linear molecules. The similarity of their electronic ground-state configurations combined with the systematic variation of the quadrupole moment and the polarisability led us to expect resemblances and differences in the electron impact spectra. Unfortunately, the permanent dipole moment of OCS disturbs the series and makes a comparison more difficult. The present paper completes the systematic investigation of the three triatomic molecules by low-energy electron spectroscopy. The results on $e^- + CO_2$ scattering have already been published by Kochem *et al* (1985a, b).

The systems $e^- + OCS$ and $e^- + CS_2$ provide the full variety of interaction mechanisms which are typical for low-energy electron scattering, i.e. direct as well as resonant and bound-state (virtual-state) collisions.

In the case of OCS the direct scattering proceeds dominantly via the dipole potential. With a permanent moment of 0.279 ea_0 (Itikawa 1970) the $e^- + OCS$ system links the studies on weakly polar (Sohn *et al* (1985) for $e^+ + CO$) and strongly polar molecules (Rohr 1977 for e^- + hydrogen halides). Furthermore, the isotropic and anisotropic polarisation potentials, which are the dominant long-range interactions for $e^- + CS_2$, increase in strength when passing from OCS to CS_2. This is indicated by the static dipole polarisabilities $\alpha_0(OCS) = 37.8$ au, $\alpha_2(OCS) = 31.1$ au, $\alpha_0(CS_2) = 59$ au and $\alpha_2(CS_2) = 43$ au, where α_0 and α_2 are the isotropic and the anisotropic polarisabilities (Landolt-Börnstein 1951). The quadrupole moments are $Q(OCS) = 2.318$ au and $Q(CS_2) = 1.346$ au (Stogryn and Stogryn 1966). Direct vibrational excitation can be characterised by the corresponding transition matrix elements. From infrared spectroscopy (Bishop and Cheung 1982) the dipole transition matrix elements are known. They range from $D = 0.0186$ au for the bending mode of OCS to 0.149 au for the asymmetric stretch mode of CS_2; as the cross sections scale with D^2 they differ by

0022-3700/87/313217+20$02.50

roughly two orders of magnitude for these two extreme cases. In addition, the mutual exclusion principle between dipole- and polarisation-induced transition holds for the linear and inversion symmetric CS_2 molecule, quite in contrast to OCS.

Resonant scattering is predicted by the calculations of Lynch *et al* (1979) to be dominant for energies above 3 eV both for OCS and CS_2. In addition, for $e^- + CS_2$ these authors predict a $^2\Pi_u$ resonance, located at 1.85 eV collision energy, with an asymptotic f-wave behaviour. Such an f-wave resonance has not been observed up to now in low-energy electron spectroscopy.

Both target systems are known to possess appreciable electron affinities between 0.4 and 1 eV (Drzaic *et al* 1984) so that the existence of a stable negative molecular ion is likely. This bound state may influence the cross sections close to threshold similar to a virtual state.

In the past, the targets OCS and CS_2 have not been studied extensively for primary electron energies below 5 eV. Experimental investigations have been published by Szmytkowski (1983) (OCS; total cross sections), Tronc and Azria (1979) (OCS; differential cross sections for elastic scattering and vibrational excitation of the symmetric stretch mode) and Ziesel *et al* (1975) (OCS and CS_2; dissociative attachment). The only theoretical studies on OCS and CS_2 have been performed by Lynch *et al* (1979). They will be discussed in § 3.

2. Experimental set-up and evaluation procedure

The measurements have been performed with a crossed beam spectrometer based on the one described by Sohn *et al* (1983). Several improvements of the experimental set-up have been carried out.

The physical dimensions of the optical systems have been reduced in order to increase the range of scattering angles to 140°. The electron gun is equipped with a differential pumping system with an effective pumping speed of 70 l s^{-1} to avoid surface contamination of the electrodes and the cathode. This contamination affects the performance of the spectrometer most severely for polar gases. The differential pumping system therefore was essential for the measurements on OCS.

The energy selection in the electron gun and in the detector system is achieved by tandem 127° cylindrical condensers with lens systems between the two condensers. Thus the two condensers can be operated at somewhat different pass energies. For the electron gun the most convenient mode of operation is the one using the first monochromator as a preselector with a typical pass energy of 1.2 eV. The second selector with a pass energy of 0.7 eV provides the proper energy selection. An energy resolution of 20 meV FWHM could be maintained during the measurements on CS_2 and of 24 meV for OCS. The double energy disperser drastically reduces the base width of the apparatus line profile. This was most useful for the separation of the bending mode peak from the elastic peak. The improved background suppression allows measurements at small scattering angles.

To improve surface properties the system is bakeable up to 550, 400 and 720 K for the electron gun, the analyser and the gas nozzle, respectively. Differential cross sections for vibrational excitation have been obtained by measuring energy loss spectra at each energy and scattering angle of interest including the elastic scattering and all vibrational transitions under consideration. If transitions could not be fully separated, the relative intensities of the transitions involved have been determined by a fitting

procedure where the peak shape has been assumed to be the apparatus profile. A possible broadening of the peaks due to rovibrational excitation is not accounted for in this procedure.

The transmission properties of the spectrometer as well as the angular correction factors are evaluated by measuring the elastic $e^- + He$ scattering rates and comparing the results with the calculated cross sections of Nesbet (1979) which are assumed to be accurate within 1%.

The absolute normalisation of the measured intensities has been performed by the flux flow method (Jung *et al* 1982) also using the $e^- + He$ elastic differential cross sections as a standard. This method requires the target beam profiles of He and the gas under consideration to be identical. These profiles have been measured by scanning a modified commercial ionisation gauge through the scattering region. The beam profiles have been found to depend on the flux rate through the nozzle. The flux rates have finally been chosen to minimise the differences in the profiles. This method of determining absolute cross sections is reliable if the energy loss is small in comparison with the primary energy. The transmission properties of the entrance optics of the electron detector was known to be rather insensitive with respect to energy variations. Therefore the cross sections are considered to be trustworthy if the energy loss does not exceed two thirds of the impact energy.

To determine integral cross sections the differential cross sections had to be extrapolated to 0 and 180°, respectively. The extrapolation procedure was guided by theoretical approximations (in most cases the first Born approximation) for the relevant process.

Statistical errors are indicated by error bars in the figures. The error of the normalisation procedure is estimated to be 15%. The inaccuracy of the procedure to obtain integral cross sections is less than 8%.

3. Results and discussion

3.1. OCS

As a survey of the low-energy $e^- + OCS$ scattering, the energy dependence of the differential elastic cross section (DCS) between 0.2 and 5 eV at the scattering angle $\vartheta = 130°$ is shown in figure 1. By comparing the result of calculations of Lynch *et al* (1979) for the integral elastic cross section, one can attribute the weak structure around 3.2 eV to the overlapping of a Δ and a Σ resonance. The more pronounced bump at 1.2 eV observed in the experiment corresponds to a Π resonance. The large increase of the cross section towards threshold is found in the experiment as well as in theory. The experimental results for the elastic and vibrationally inelastic scattering are now discussed in more detail within the three energy regions mentioned above.

3.1.1. Scattering via the Δ, Σ resonances. Figure 2 shows a typical energy loss spectrum for the energy region between 3 and 5 eV. The elastic scattering is dominant and one observes the excitation of all three fundamental modes of vibration (bending mode (010): vibrational energy quantum $E_{010} = 64$ meV; symmetric stretch mode (100): $E_{100} = 107$ meV; asymmetric stretch mode (001): $E_{001} = 256$ meV). In addition, the first overtone of the symmetric stretch mode is also excited. The excitation of the symmetric

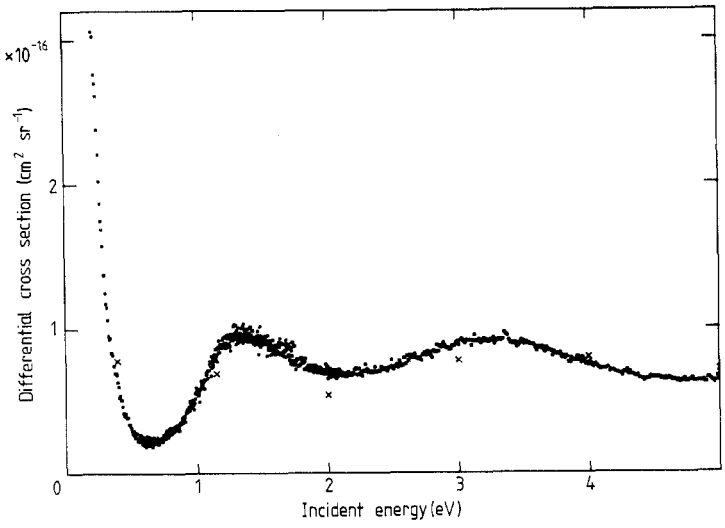

Figure 1. Energy dependence of the elastic DCS for $e^- + OCS$ at 130° scattering angle. The crosses are taken from independently measured angular dependences.

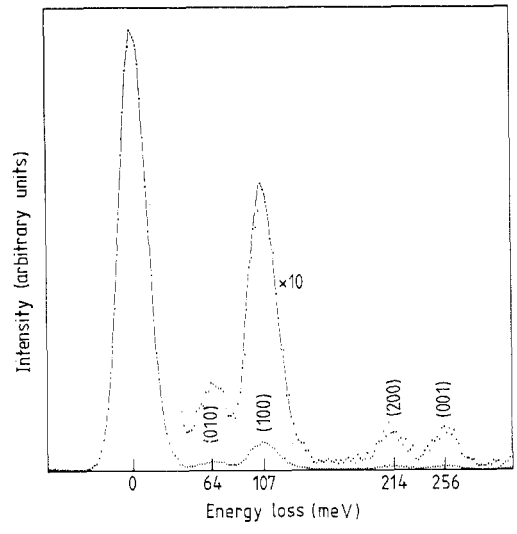

Figure 2. Energy loss spectrum for $e^- + OCS$ scattering at 4 eV primary energy and a scattering angle of 138°.

stretch mode is the dominant inelastic process. In figure 3 angular dependences of the elastic DCS and the (010), (100), (200) and (001) mode excitation cross sections for a collision energy of 4 eV are plotted. The elastic DCS exhibits a weak d-wave structure with a minimum at a scattering angle of about 120° which indicates the resonant scattering. Apart from the asymmetric stretch vibration the vibrational excitation cross sections show a rather flat angular distribution suggesting that the Σ resonance dominates over the Δ resonance in this energy region provided both resonances are asymptotically of d-wave type. Although the resonances seem to be weak at first sight, their effect on the vibrational excitation is remarkable. This can be seen from figure

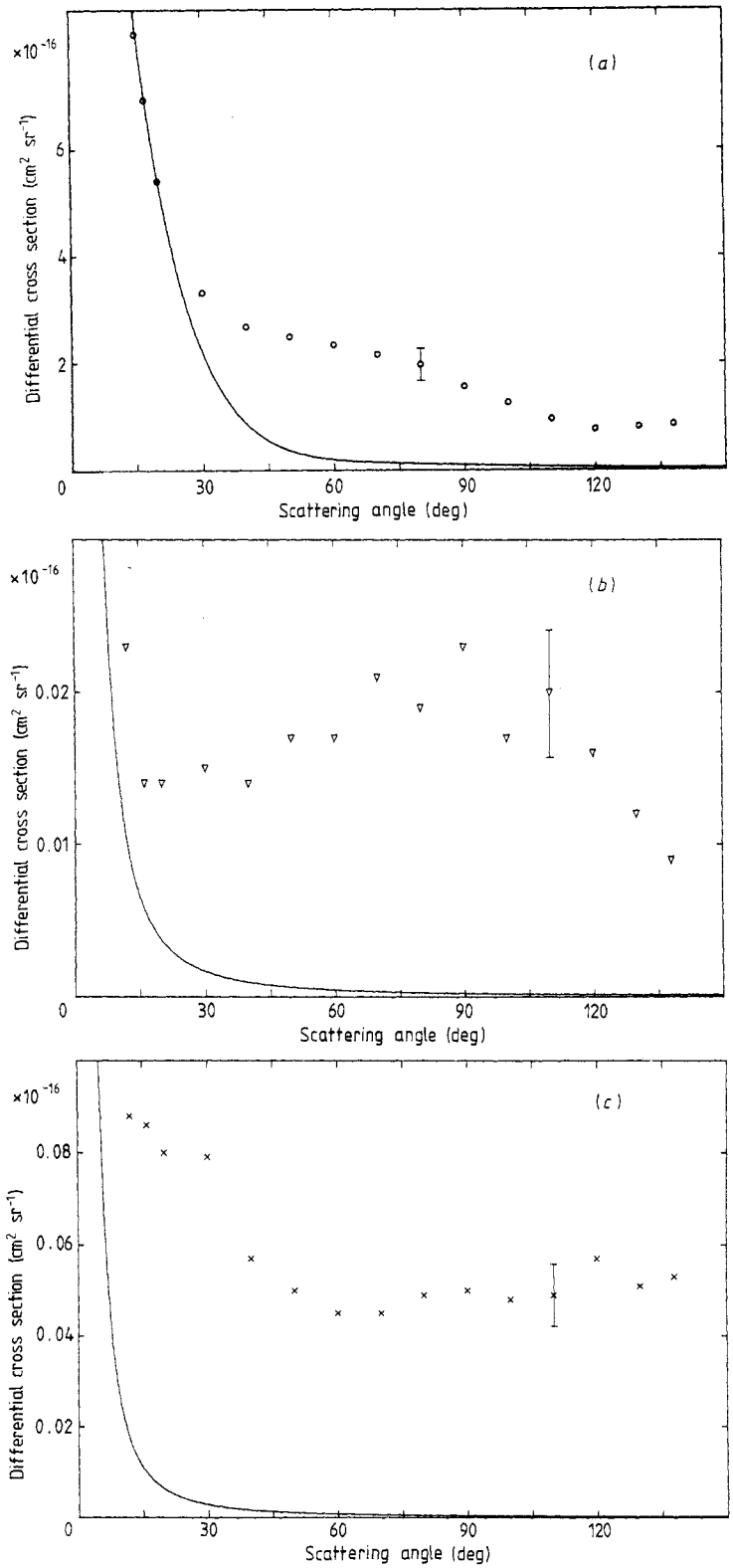

Figure 3. Angular dependences of the DCS for $e^- + OCS$ for (*a*) elastic scattering and vibrational excitation of the (*b*) (010), (*c*) (100), (*d*) (200) and (*e*) (001) modes in the Σ, Δ resonance region (4 eV). ——, Born dipole approximation.

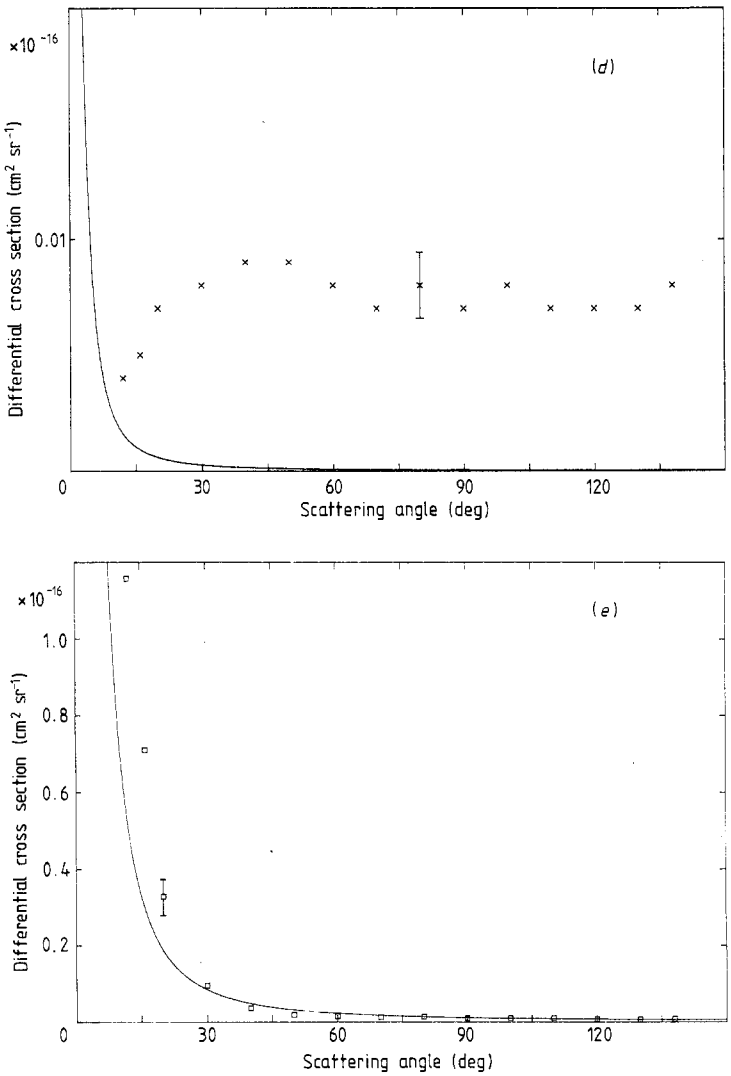

Figure 3. (continued)

3, where the measured DCS are compared with the predictions of the first Born dipole approximation (full curve in figure 3) which should represent the main direct contribution to the cross section

$$\frac{d\sigma}{d\Omega} = \frac{4}{3} D^2 \frac{k_f}{k_i} \frac{1}{k^2}$$

where $k_f(k_i)$ is the final (initial) momentum of the projectile, D is the dipole transition matrix element and k is momentum transfer (all numbers in atomic units).

The corresponding matrix elements are $D_{010} = 0.0186$ au, $D_{100} = 0.0268$ au, $D_{200} = 0.008$ au and $D_{001} = 0.134$ au (Bishop and Cheung 1982). Apart from the small angle scattering, the observed cross sections differ from the first Born predictions by orders of magnitude. This is partly due to the relatively small transition matrix elements so

that even a weak resonance clearly enhances the excitation cross sections. The differential cross sections for the excitation of the asymmetric stretch mode behave quite differently. This mode is not distinctly affected by the resonance.

3.1.2. Scattering via the Π resonance. At 1.15 eV collision energy—just in the maximum of the Π resonance—the situation is totally different. Figure 4 shows two energy loss spectra taken at this energy for 30 and 90° scattering angles. Vibrational excitation is very pronounced. The bending mode is strongly excited and several overtones and intercombinations are clearly visible. In addition, excitation of several combination tones occurs. The dominance of the (0n0) mode is a hint for a bent structure of the resonance configuration.

The experimental results on the Π-resonance scattering and the calculations of Lynch *et al* (1979) show some differences. The resonance is found to possess a half

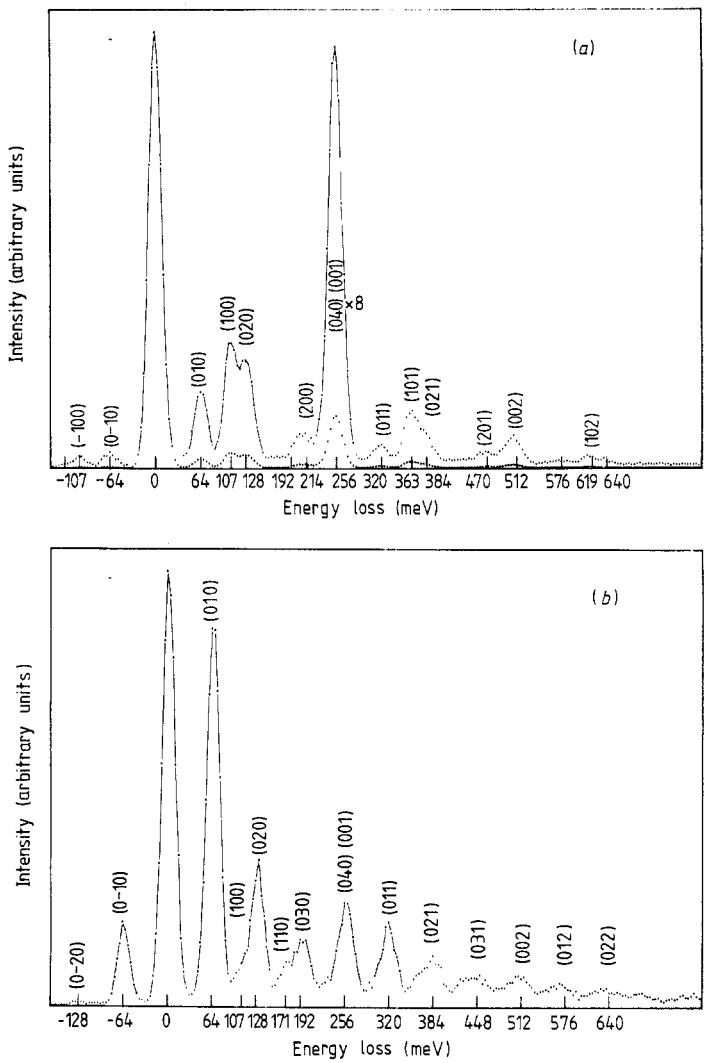

Figure 4. Energy loss spectra for OCS for a collision energy of 1.15 eV and (*a*) 30 and (*b*) 90° scattering angle.

width of about 0.8 eV whereas the theory predicts 0.12 eV. This difference may come from the suppression of vibrational excitation exit channels in the work of Lynch *et al*; the experiment shows that the decay of the resonant state into the vibrational channels is appreciable.

In the calculations the asymptotic partial wave for the Π-resonance scattering has been determined to be a d wave whereas the experimental results of this work and of Tronc and Azria (1983) are more consistent with a dominant p wave (see figure 5).

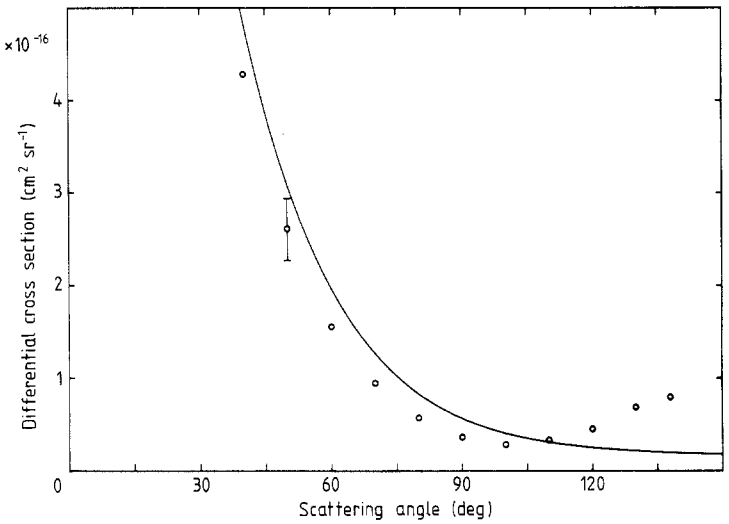

Figure 5. Angular dependence of the elastic DCS for OCS at 1.15 eV.

Despite these differences between theory and experiment the occurrence of the predicted resonance around the calculated energy is satisfactory if one realises that Lynch *et al* quote their results to be 'realistic survey calculations' for this scattering system.

3.1.3. Threshold behaviour. In the energy region below 0.8 eV the scattering process should not be affected by resonances (see figure 1). However, the energy loss spectrum at 0.4 eV (figure 6) shows some unexpected features. One observes strong excitation of bending mode overtones. For lower scattering angles the (020) excitation cross section exceeds the (010) mode. The symmetric stretch excitation is weak and hidden in the low-energy wing of the (020) peak. In figure 7 angular dependences of the elastic DCS and the DCS for vibrational excitation of the (010) and (001) mode at 0.6 eV are shown, again compared with the Born approximation. For vibrational excitation only the dipole approximation is used. For the calculation of the elastic scattering the dipole, the quadrupole, the isotropic and anisotropic polarisation potentials have been taken into account. The Born dipole approximation describes the experimental results for the asymmetric stretch mode correctly in shape but underestimates the absolute cross sections. Theory however fails to reproduce the measured angular behaviour for the bending mode. The observed backscattering is in contradiction to the model of dipole-induced transitions. In the Born approximation excitation via the anisotropic polarisation potential leads to angular distributions with their maxima in the backward

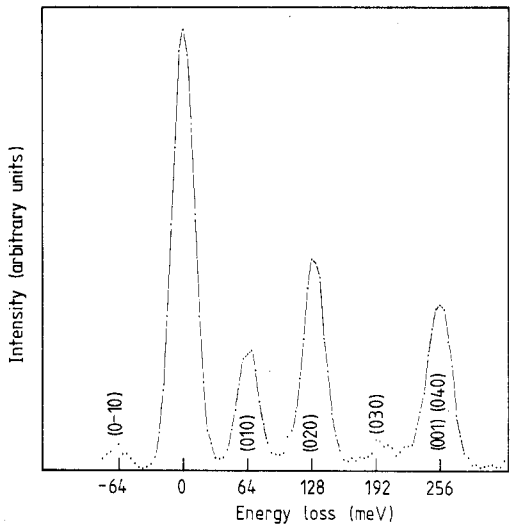

Figure 6. Energy loss spectrum for OCS for a collision energy of 0.4 eV and 138° scattering angle.

direction, but to fit the data the corresponding transition matrix element had to be of the order of 10 au which is not realistic. The model of direct interactions can explain the elastic scattering in the threshold energy region, but some questions remain about the nature of the vibrational excitation mechanisms. A possible bound state of the $e^- + OCS$ system may be responsible for these peculiarities.

We do not think that the unusual angular dependences of the bending vibration, as shown in figure 7(*b*), are experimental artefacts because the energy loss ΔE (64 meV) is small in comparison with the collision energy E_0 (0.6 eV). The data for the asymmetric stretch vibration with an even larger energy loss monotonically decrease with increasing angle as expected.

3.1.4. Integral and total cross sections. In table 1 the integral cross sections for elastic scattering and vibrational excitation of the fundamental modes are listed for all primary energies under consideration together with the total cross sections. Note again that for 1.15 eV (Π resonance) the total vibrational cross section is more than 40% of the integral elastic cross section so that the maximum of the total cross section is mainly caused by the resonant enhancement of vibrational excitation. The cross section for dissociative attachment has been determined by Ziesel *et al* (1975) to be 0.29×10^{-17} cm^2 and is therefore of minor importance for the total cross section.

The total and integral cross sections are finally compared in figure 8 with the calculations of Lynch *et al* (1979) and the experimental results for the total cross section determined by Szmytkowski (1983). Good agreement is found for energies above 1 eV, whereas differences remain in the threshold region. The disagreement between the results of Lynch *et al* and this work may come from the neglection of the long-range part of the interaction potential (dipole, polarisation potential) in the calculations.

Finally, the full set of measured DCS for $e^- + OCS$ scattering is tabulated in tables 2 (elastic scattering) and 3 (vibrational excitation).

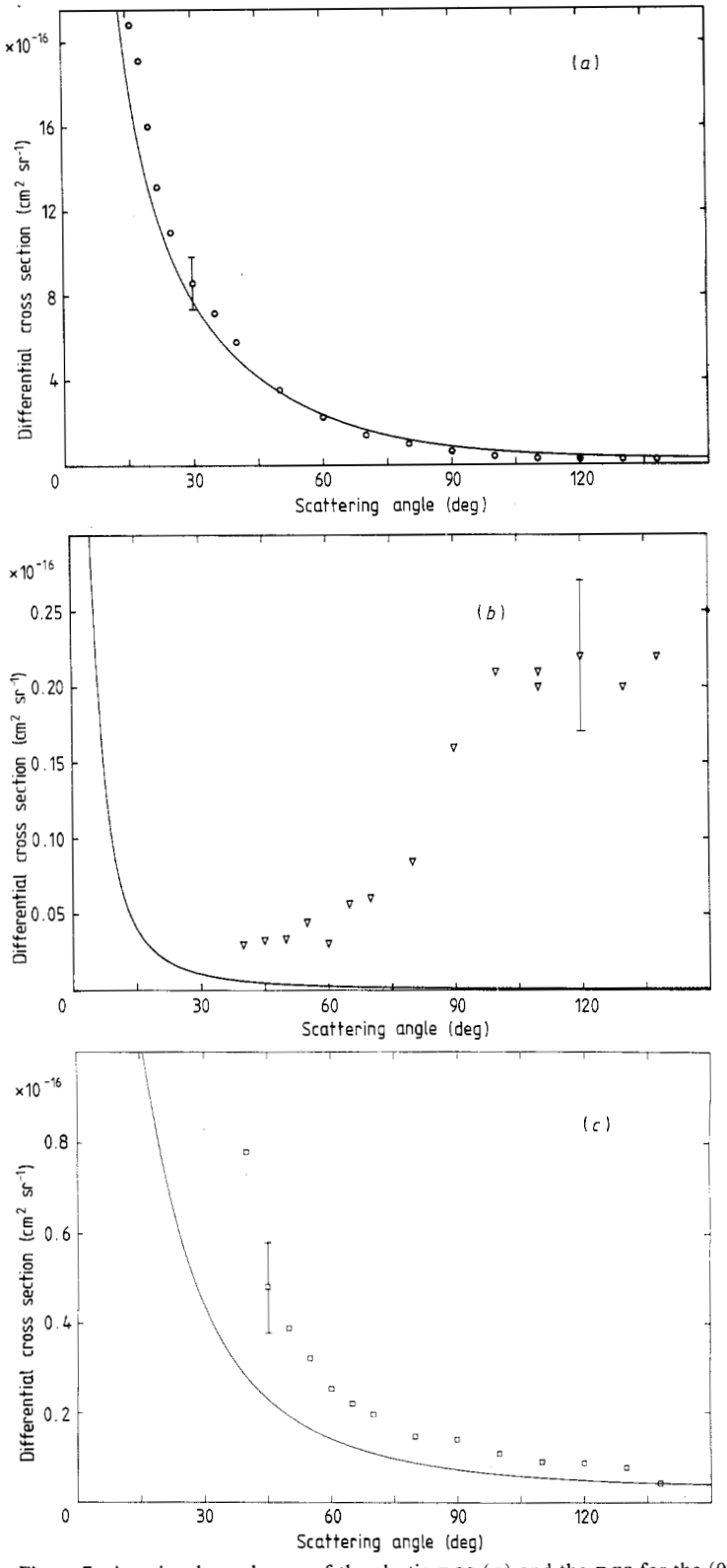

Figure 7. Angular dependences of the elastic DCS (*a*) and the DCS for the (010) (*b*) and (001) (*c*) excitations for OCS. The primary electron energy is 0.6 eV. In the case of elastic scattering, the cut-off radius for the polarisation potential has been fitted to 6 a_0, in reasonable agreement with the size of the molecule ($\simeq$4.5 a_0). The full curves show the results of the Born dipole approximation.

Table 1. Integral cross sections for $e^- + OCS$ elastic scattering and vibrational excitation. The total cross section and the total vibrational cross section are also tabulated. All cross sections are given in 10^{-16} cm^2.

Energy (eV)	Total	Elastic	010	100	001	Vibrational
0.4	—	57.2	—	—	—	—
0.6	46.05	39.4	3.65	—	3	6.65
1.15	51.5	36.1	9.6	2	3.8	15.4
1.7	—	18.9	—	—	—	—
2	—	16.9	—	—	—	—
2.5	17	15.3	0.3	0.6	0.82	1.7
3	20.9	19.6	0.27	0.4	0.62	1.3
3.5	24.5	23	0.28	0.6	0.63	1.5
4	28.1	26.3	0.25	0.84	0.69	1.8
5	—	25.8	—	—	—	—

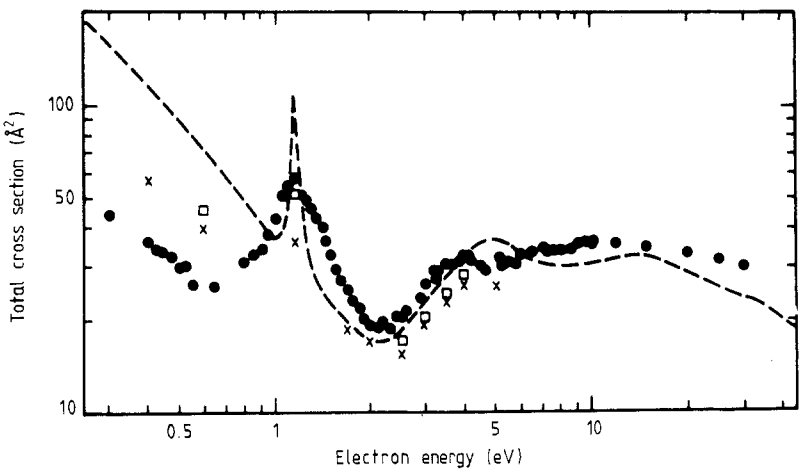

Figure 8. Integral elastic and total cross sections for $e^- + OCS$. - - -, Lynch *et al* (1979) (integral elastic); •••, Szmytkowski (1983) (total); × × ×, this work (integral elastic); □□□, this work (total).

3.2. CS_2

3.2.1. Elastic scattering. If one compares the energy dependence of the elastic DCS for 130° scattering angle (figure 9) with the integral elastic cross sections calculated by Lynch *et al* (1979), the overall agreement between theory and experiment is found to be worse than in the $e^- + OCS$ case. The most striking discrepancy is the absence of a resonant structure in the measured energy dependence which could correspond to a theoretically predicted $^2\Pi_u$ resonance at 1.85 eV collision energy with a dominant f partial wave. The measured angular dependences (figure 10 and table 6) show a dominant d-wave behaviour in the energy range between 0.8 and 5 eV. Therefore our work does not support the existence of a $^2\Pi_u$ resonance for the $e^- + CS_2$ scattering. Unpublished measurements of the total cross section performed by Szmytkowski 1985 also give no hints for a resonance in this energy region.

The large enhancement of the elastic DCS (see figure 9) towards higher energies may be attributed to overlapping Σ_u and Δ_g resonances. As mentioned above this

Table 2. DCS (10^{-16} cm^2 sr^{-1}) for elastic $e^- + OCS$ scattering.

	E(eV)									
ϑ	0.4	0.6	1.15	1.7	2	2.5	3	3.5	4	5
138	0.61	0.24	0.80	0.97	0.54		0.83		0.85	0.87
130	0.78	0.25	0.69	0.89	0.54		0.78		0.80	0.71
120	0.90	0.27	0.45	0.76	0.54		0.73		0.76	0.66
110		0.30	0.33	0.59			0.85		0.95	0.78
105	1.22				0.66	0.68		1.19		
100		0.41	0.28	0.71			1.05		1.25	1.13
90	1.78	0.65	0.36	0.69	0.88	1.10	1.32	1.54	1.56	1.44
80		1.00	0.57	0.79			1.51		1.97	1.79
75	2.41				1.08	1.40		1.82		
70		1.42	0.95	0.95			1.51		2.16	2.12
60	3.43	2.26	1.56	1.14	1.08	1.32	1.54	1.95	2.34	2.35
50	4.51	3.54	2.61	1.25	1.01		1.43		2.49	2.64
45						1.00		1.89		
40	6.33	5.81	4.28	1.31	0.94		1.32		2.68	3.16
35	7.81	7.18				0.90		1.85		
30	9.86	8.60	6.97	1.54	1.27	0.93	1.73	2.02	3.31	3.89
27	11.38		9.59							
25	12.98	10.98	11.46		1.98	1.09	2.51	2.34		
22	18.53	13.14					3.25			
20	23.08	16.02		2.79	3.87	1.88	4.45	3.13	5.41	5.39
18		19.13								
17				3.19	5.67				6.93	6.80
16		20.81								
15				4.48	7.50	3.57		4.28	8.15	7.98
13					10.13					

resonance structure is found to be d-wave dominated and extends from 0.8 eV up to the highest energies investigated. With the assumption that the leading phases of each symmetry are responsible for the resonance, the resonant phaseshifts $\delta_{l\lambda}$ should be $\delta_{p\sigma}$ for Σ_u and $\delta_{d\delta}$ for Δ_g. For the elastic scattering with its d-wave dominance the Δ_g resonance seems to be most important in this energy range.

In the energy range below 0.8 eV the elastic DCS shows a steep increase towards threshold. This may be due to a possible bound or virtual state of the $e^- + CS_2$ system. In addition, the failure of the Born approximation to fit the measured angular dependences in this energy region over an extended angular range supports this assumption. To obtain some more information about this low-energy behaviour a phaseshift analysis has been performed for the body-frame phases $\delta_{l\lambda}$ with $l \leqslant 2$ for energies less than or equal to 1.2 eV. Following Chang and Fano (1972) the DCS is given as

$$\frac{d\sigma}{d\Omega} = \frac{1}{k^2} \sum_{ll'\lambda\lambda'} \left(\frac{2}{1+\delta_{\lambda 0}}\right)\left(\frac{2}{1+\delta_{\lambda' 0}}\right)(l\lambda 00/l\lambda)(l'\lambda' 00/l'\lambda')$$

$$* 4\pi\theta(0, ll'l', \vartheta) \exp[i(\delta_{l\lambda} - \delta_{l'\lambda'})] \sin \delta_{l\lambda} \sin \delta_{l'\lambda'}$$

The Clebsch–Gordan coefficients $(l\lambda 00/l\lambda)$ and $(l'\lambda' 00/l'\lambda')$ together with the standard angular functions θ can be evaluated with the help of tables 1 and 2 in Chang (1977). The phaseshifts are obtained by fitting the theoretical expression for the DCS to the experiment and they are listed in table 4. An example of a fitted angular dependence

Table 3. DCS (10^{-16} cm^2 sr^{-1}) for the vibrational excitation of OCS by electron impact.

	E(eV)												
	(010) Bending mode			(020) Bending mode	(100) Symmetric stretch mode			(200)	(001) Asymmetric stretch mode				
ϑ	0.6	3	4	0.6	3	3.5	4	4	0.6	2.5	3	3.5	4
138	0.22	0.016	0.009	0.150	0.028		0.053	0.008	0.043		0.007		0.008
130	0.20	0.021	0.012	0.154	0.029		0.051	0.007	0.078		0.010		0.007
120	0.22	0.017	0.016	0.215	0.031		0.057	0.007	0.088		0.012		0.007
110	0.20	0.023	0.020	0.231	0.028		0.049	0.007	0.091		0.01		0.010
105						0.047				0.014		0.024	
100	0.21	0.024	0.017	0.236	0.027		0.042	0.008	0.109		0.007		0.010
90	0.16	0.027	0.023	0.174	0.034	0.050	0.050	0.007	0.140	0.014	0.007	0.026	0.010
80	0.085	0.022	0.019	0.145	0.031		0.049	0.008	0.147		0.006		0.014
75						0.042				0.014		0.031	
70	0.061	0.021	0.021	0.159	0.025		0.045	0.007	0.196		0.008		0.013
65	0.057			0.160					0.220				
60	0.031	0.019	0.017	0.165	0.026	0.042	0.045	0.008	0.253	0.025	0.009	0.030	0.015
55	0.045			0.141					0.322				
50	0.034	0.022	0.017	0.127	0.027		0.050	0.009	0.389		0.016		0.019
45	0.033			0.145		0.045			0.482	0.056		0.041	
40	0.030	0.016	0.014	0.150	0.024		0.057	0.009	0.78		0.039		0.037
35						0.042				0.122		0.061	
30		0.014	0.015		0.030	0.051	0.079	0.008		0.155	0.102	0.087	0.096
28													
25		0.014			0.037	0.044				0.267	0.183	0.129	
22		0.012			0.038						0.277		
20		0.017	0.014		0.045	0.057	0.080	0.007		0.423	0.370	0.220	0.328
18													
16			0.014				0.086	0.005					0.710
15						0.049				0.703		0.378	
12			0.023				0.088	0.004					1.158
10										1.678		0.789	
5										3.64		1.48	

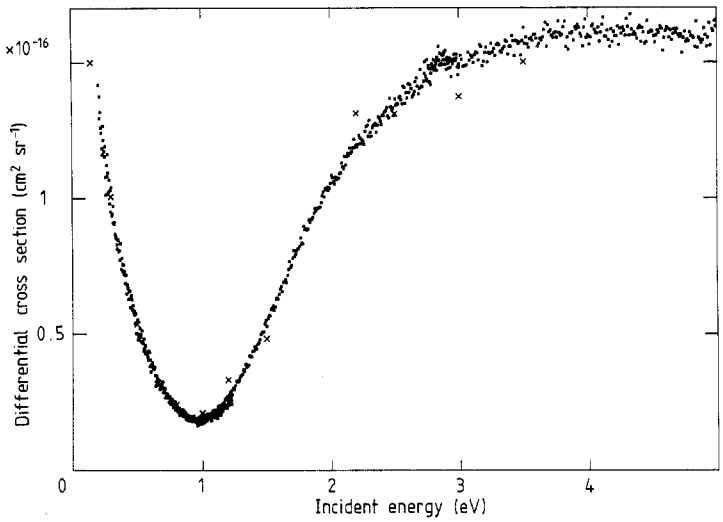

Figure 9. Energy dependence of the elastic DCS for CS_2 at 130° scattering angle. The crosses indicate results of independent angular dependence measurements.

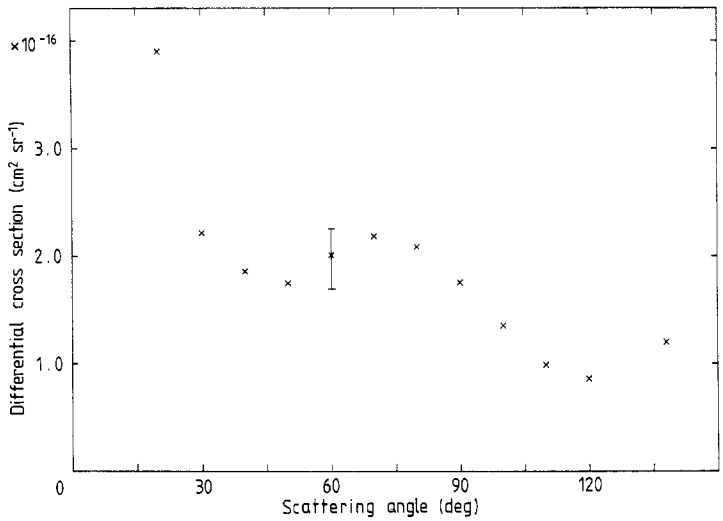

Figure 10. Angular dependence of the elastic DCS for CS_2 at 1.8 eV primary energy.

Table 4. Phaseshifts $\delta_{l\lambda}$(rad) obtained by a fit to the measured angular dependences of the elastic $e^- + CS_2$ scattering in the energy range 0.3 eV–1.2 eV.

	E(eV)				
$l\lambda$	0.3	0.5	0.8	1	1.2
00	0.049	0.111	0.124	0.194	0.157
10	0.254	0.216	0.187	0.381	0.578
11	0.087	0.083	0.079	0.042	0.022
20	−0.323	−0.420	−0.589	−0.686	−0.711
21	0.076	0.102	0.050	0.050	0.050
22	0.100	0.100	0.100	0.100	0.100

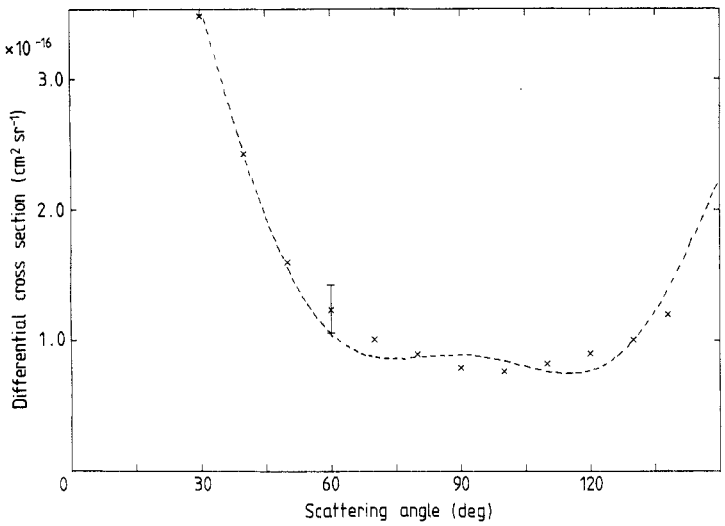

Figure 11. Angular dependence of the elastic DCS for CS_2 at 0.3 eV primary energy. × × ×, experiment; - - -, results of the phaseshift analysis.

is shown in figure 11. As higher partial waves than the d wave become more and more important with increasing primary energy the fits have been performed only up to 1.2 eV. (Contributions from higher partial waves to the DCS cannot be given in a closed form, in contrast to electron-atom scattering, where this contribution is known to scale with α^2. As α is large for CS_2 one may assume that even in the energy range less than or equal to 1.2 eV the neglect of partial waves with $l>2$ may be compensated by an overestimation of the $l=2$ phase shifts in the fit.) The phaseshift analysis shows that in the energy region between 0.3 and 1.2 eV the dominant contributions are due

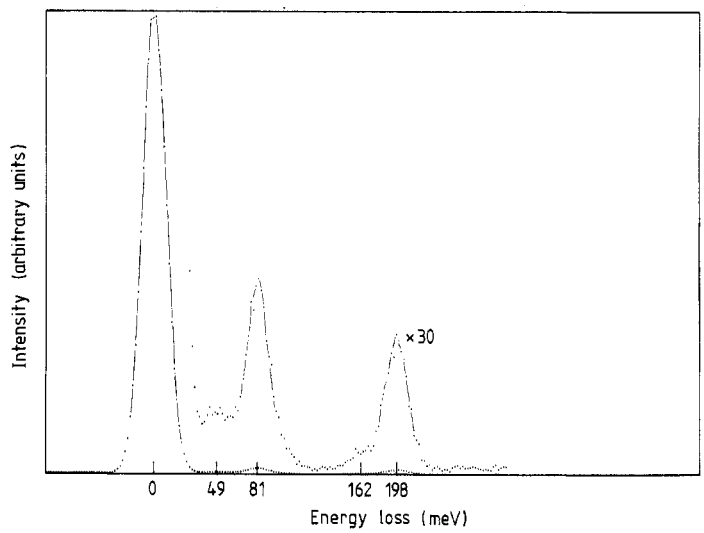

Figure 12. Energy loss spectrum for $e^- + CS_2$ scattering. The collision energy is 3.5 eV and the scattering angle is 40°.

to $\delta_{p\sigma}$ and $\delta_{d\sigma}$. The $\delta_{p\sigma}$ phase belongs to the Σ_u symmetry which yields, provided that the $^2\Pi_u$ resonance does not exist, an important contribution also in the calculations of Lynch *et al.* The $\delta_{s\sigma}$ phase should be most influenced by the bound state of $e^- + CS_2$, but is found to be of minor importance in the fits. It can therefore be stated that even at the lowest primary energy of 0.3 eV the influence of the bound state on the elastic scattering is small. The large increase of the Σ_g partial cross section is obviously due to higher partial waves (mainly $\delta_{d\sigma}$) even at energies as low as 0.3 eV. The phaseshift analysis yields $\delta_{d\sigma}$ to be the most important $l = 2$ phase, whereas the calculations of Lynch *et al* make a dominant $\delta_{d\delta}$ more probable. As the different $\delta_{d\lambda}$ phases lead to very similar angular dependences of the corresponding DCS it is difficult to fix them

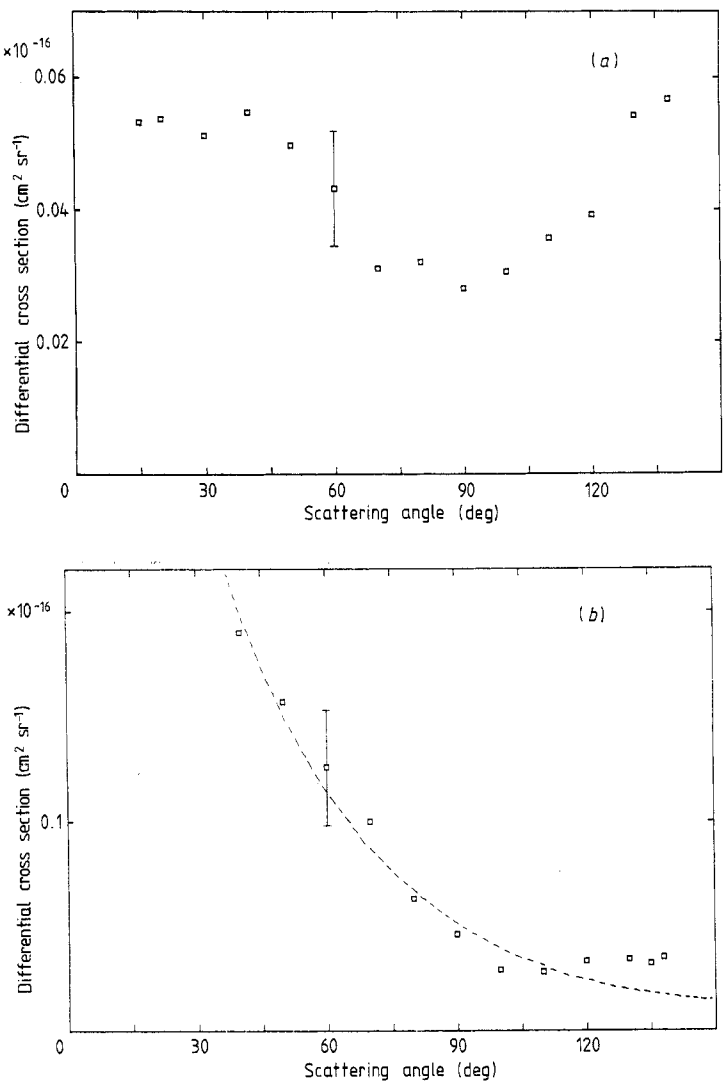

Figure 13. Angular dependences for the (100) mode excitation cross section at 3.5 (*a*) and 0.3 (*b*) eV collision energy for CS_2. □□□, experiment; - - -, Born polarisation approximation $M_\alpha = 9.5$ a.u., $r_c = 7$ a.u.

relative to each other in the fit. Actually one may fix $\delta_{d\sigma}$ to zero in the fit and one then ends up with a slightly worse fit with $\delta_{d\delta}$ dominant.

3.2.2. Vibrational excitation. The three fundamental modes of vibration of CS_2 are the bending mode ($\Delta E = 0.049$ eV), the symmetric stretch mode ($\Delta E = 0.081$ eV) and the asymmetric stretch mode ($\Delta E = 0.190$ eV). Figure 12 shows a typical energy loss spectrum for low-energy $e^- + CS_2$ scattering. The vibrational excitation cross sections are small relative to the elastic cross section over the whole energy and angular range investigated. For primary energies above 1 eV only the excitation of the fundamental modes is observed; in the very low-energy region the first overtone of the bending mode is clearly visible in the energy loss spectra. This is in full analogy with $e^- + OCS$ scattering. The infrared active vibrations show an excitation cross section behaviour very similar to the $e^- + OCS$ case. The main difference between both targets is again

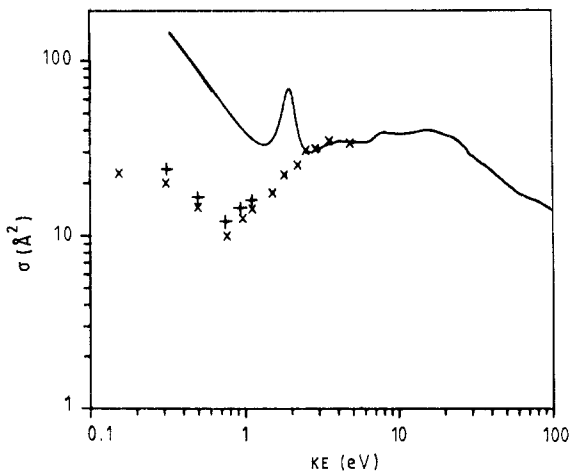

Figure 14. Energy dependence of the integral elastic cross section for $e^- + CS_2$, ×××, this work; ——, Lynch *et al* (1979).

Table 5. Integral cross sections for $e^- + CS_2$ elastic scattering, and vibrational excitation in 10^{-16} cm^2. For comparison the results from the first Born approximation are also given.

E(eV)	Elastic	100	010 Exp	010 Born	001 Exp	001 Born	Total
0.3	18.7	1.06	2.02	0.26	3.26	3.31	25.04
0.5	12.8	0.40	0.79	0.18	2.62	3.01	16.61
0.8	9.5	0.14	0.61	0.13	1.67	2.38	11.92
1	12.3	0.11	0.55	0.11	1.73	2.08	14.68
1.2	14.9	0.09	0.49	0.09	1.54	1.85	17.02
1.5	17.3	0.11	0.37	0.08	1.28	1.59	19.06
1.8	22.4	0.12	0.24	0.07	1.07	1.41	23.83
2.2	25.4	0.26	0.27	0.06	1.01	1.22	29.95
3	31.6	0.41	0.23	0.05	0.84	0.97	33.08
3.5	35.5	0.54	0.29	0.04	0.83	0.86	37.16
5	35.1	0.23	0.35	0.03	0.70	0.66	36.38

Table 6. DCS for $e^- + CS_2$ elastic scattering and excitation of the fundamental modes of vibration. All cross sections are given in 10^{-16} cm^2.

	E_0(eV)										
ϑ	0.3	0.5	0.8	1	1.2	1.5	1.8	2.2	3	3.5	5
CS_2 elastic											
12.5	—	—	—	—	—	—	—	5.166	—	—	
15	—	—	—	—	3.751	3.737	—	4.502	6.108	8.835	10.179
17	—	—	—	—	3.163	3.244	—	—	5.607	—	9.107
20	—	3.619	1.936	3.059	3.048	2.831	3.899	3.510	5.008	6.721	8.283
30	3.478	2.257	1.166	1.547	1.827	1.759	2.217	2.380	3.457	4.290	5.982
40	2.426	1.522	0.781	1.019	1.190	1.501	1.859	2.228	3.074	3.786	4.550
50	1.596	1.038	0.711	1.036	1.272	1.739	1.748	2.423	3.136	3.818	3.700
60	1.234	0.900	0.793	1.251	1.447	1.951	2.011	2.581	3.132	3.601	3.119
70	1.009	0.835	0.857	1.343	1.628	1.935	2.185	2.521	2.989	2.949	3.054
80	0.897	0.803	0.977	1.211	1.543	1.757	2.086	2.148	2.531	2.775	2.739
90	0.792	0.675	0.678	0.944	1.253	1.397	1.754	1.612	2.057	2.353	1.979
100	0.763	0.590	0.502	0.623	0.865	1.001	1.354	1.350	1.726	1.929	1.573
110	0.821	0.524	0.362	0.357	0.558	0.625	0.988	1.110	1.435	1.608	1.110
120	0.901	0.524	0.233	0.217	0.349	0.441	0.858	1.085	1.303	1.452	0.901
130	1.006	0.535	0.239	0.208	0.331	0.483	—	1.312	1.374	1.502	1.024
138	1.199	0.587	0.320	0.291	0.474	0.728	1.200	1.675	1.630	1.575	1.298
CS_2 bending mode											
12.5	—	—	—	—	—	—	—	0.044	—	—	—
15	—	—	—	—	0.076	0.056	0.064	0.0337	0.0302	0.0266	0.0103
17	—	—	—	—	0.057	0.042	—	—	—	—	—
20	—	—	0.096	0.067	0.043	0.031	0.033	0.0211	0.0173	0.0166	0.0125
30	0.19	0.045	0.019	0.018	0.013	0.0139	0.01	0.0142	0.0103	0.0131	0.0149
40	0.086	0.012	0.011	0.01	0.0096	0.0119	0.005	0.0133	0.0123	0.0131	0.0229
50	0.019	0.01	0.014	0.016	0.014	0.0155	0.009	0.0159	0.0140	0.0171	0.0298
60	0.0126	0.022	0.028	0.027	0.021	0.0193	0.013	0.0188	0.0171	0.0181	0.0313
70	0.036	0.038	0.036	0.043	0.031	0.0231	0.014	0.0202	0.0184	0.0206	0.0384
80	0.06	0.052	0.057	0.044	0.038	0.0317	0.018	0.0236	0.0188	0.0236	0.0414
90	0.048	0.067	0.058	0.052	0.045	0.0335	0.018	0.0209	0.0173	0.0271	0.0369
100	0.058	0.077	0.056	0.050	0.046	0.0359	0.020	0.0202	0.0171	0.0281	0.0331
110	0.084	0.094	0.053	0.050	0.049	0.0299	0.019	0.0202	0.0171	0.0251	0.0284
120	0.107	0.089	0.052	0.044	0.048	0.0273	0.019	0.0189	0.0156	0.0241	0.0253
130	0.128	0.0854	0.051	0.042	0.044	0.0231	—	0.0196	0.0164	0.0256	0.0226
138	0.167	0.0761	0.0493	0.044	0.039	0.0275	0.018	0.0225	0.0184	0.0236	0.0194
CS_2 symmetric stretch											
15	—	—	—	—	—	—	—	—	—	0.0532	0.0203
17	—	—	—	—	—	—	—	—	—	—	—
20	—	—	0.0418	—	0.021	0.0168	0.017	0.0263	0.0421	0.0537	0.0191
30	—	0.09	0.0345	0.034	0.023	0.0210	0.0126	0.0233	0.0429	0.0512	0.0208
40	0.19	0.091	0.0267	0.026	0.017	0.0133	0.0105	0.0223	0.0397	0.0547	0.0229
50	0.157	0.067	0.0214	0.016	0.011	0.0119	0.0093	0.0193	0.0388	0.0497	0.0185
60	0.126	0.054	0.0153	0.013	0.0088	0.0077	0.0081	0.0181	0.0311	0.0432	0.0188
70	0.100	0.033	0.0107	0.0081	0.0058	0.0075	0.0071	0.0176	0.0276	0.0311	0.0167
80	0.063	0.021	0.0089	0.0048	0.0046	0.0086	0.0081	0.0182	0.0227	0.0321	0.0164
90	0.046	0.011	0.0049	0.0028	0.0032	0.0068	0.0093	0.0193	0.0227	0.0281	0.0158
100	0.029	0.0053	0.0029	0.0019	0.0035	0.0079	0.0091	0.0188	0.0257	0.0306	0.0188
110	0.028	0.0042	0.0088	0.0017	0.0039	0.0066	0.0095	0.0183	0.0255	0.0357	0.0179
120	0.033	0.0052	0.0011	0.0011	0.0021	0.0055	0.0095	0.0189	0.0298	0.0392	0.0173
130	0.034	0.0064	0.0017	0.001	0.0017	0.0053	0.0099	0.0223	0.0354	0.0542	0.0185
138	0.035	0.007	0.0029	0.0015	0.0019	0.0044	—	0.0243	0.0438	0.0567	0.0194

Table 6. (continued)

	E_0(eV)										
ϑ	0.3	0.5	0.8	1	1.2	1.5	1.8	2.2	3	3.5	5
CS_2 assymmetric stretch											
15	—	—	—	—	—	—	—	0.492	—	—	0.185
17	—	—	—	—	—	—	—	—	—	—	—
20	—	—	—	—	0.750	0.486	0.471	0.280	0.264	0.215	0.104
30	—	—	0.823	0.456	0.351	0.228	0.132	0.111	0.082	0.064	0.049
40	0.571	0.486	0.411	0.193	0.150	0.111	0.063	0.058	0.037	0.038	0.030
50	0.503	0.269	0.193	0.104	0.085	0.061	0.031	0.036	0.023	0.029	0.027
60	0.361	0.180	0.112	0.069	0.047	0.039	0.020	0.031	0.021	0.031	0.026
70	0.262	0.125	0.066	0.047	0.034	0.027	0.014	0.025	0.021	0.027	0.028
80	0.163	0.088	0.045	0.025	0.023	0.021	0.013	0.026	0.020	0.025	0.030
90	0.115	0.064	0.027	0.018	0.016	0.0166	0.013	0.021	0.018	0.023	0.026
100	0.093	0.053	0.019	0.013	0.015	0.012	0.011	0.019	0.016	0.021	0.023
110	0.087	0.042	0.0165	0.010	0.013	0.0104	0.0098	0.018	0.014	0.018	0.020
120	0.081	0.031	0.0145	0.008	0.008	0.0082	0.0086	0.017	0.012	0.018	0.021
130	0.078	0.024	0.0133	0.007	0.0075	0.0086	—	0.016	0.012	0.018	0.026
138	0.085	0.018	0.012	0.008	0.007	0.0093	0.018	0.0099	0.014	0.021	0.031

the fact that the II resonance does not exist for the CS_2 molecule. For the interpretation of the observed (010) and (001) excitation and for the comparison between experiment and the first Born dipole approximation the same arguments as for the $e^- + OCS$ scattering hold.

The angular dependences for the excitation of the infrared inactive symmetric stretch vibration are nearly isotropic for higher energies and change to a prominent forward scattering at low collision energies (see figure 13). The latter is qualitatively consistent with the predictions of the Born polarisation approximation. A more detailed comparison shows however that the polarisation transition matrix element M_α that fits the experimental result at 0.3 eV amounts to 9.5 au. From Raman spectroscopy data (Murphy *et al* 1969) one can roughly estimate the actual matrix element to 1.2 au, quite in contrast to the fitted value. In addition, the set of parameters M_α and r_c (cut-off radius of the polarisation potential) determined for a given primary energy does not fit the experiment for the neighbouring energies investigated. As the (100) excitation also shows a steep increase towards threshold energies, the model of a direct scattering mechanism seems inadequate. An enhanced excitation due to a bound state of the $e^- + CS_2$ system is most probable, despite the apparent anisotropic low-energy angular behaviour.

3.2.3. Integral and total cross sections. In table 5 the integral elastic, integral vibrational excitation and total cross sections for the $e^- + CS_2$ scattering are listed. The integral elastic cross section is finally compared with the theoretical results of Lynch *et al* in figure 14. Obviously, the $^2\Pi_u$ resonance, which leads to an enhancement of the cross section by more than a factor two with a halfwidth of about 0.3 eV, is totally absent in the experimental data.

The DCS for elastic scattering and vibrational excitation are finally summarised in table 6.

Acknowledgment

This work has been supported by the Deutsche Forschungsgemeinschaft under SFB 91.

References

Bishop D M and Cheung L M 1982 *J. Phys. Chem. Ref. Data* **11** 119
Chang E S 1977 *Phys. Rev.* A **16** 1841
Chang E S and Fano U 1972 *Phys. Rev.* A **6** 173
Drzaic P S, Marks J and Brauman J I 1984 *Gas Phase Ion Chem.* **3** 167
Itikawa Y 1970 *J. Phys. Soc. Japan* **28** 1062
Jung K, Antoni Th, Müller R, Kochem K-H and Ehrhardt H 1982 *J. Phys. B: At. Mol. Phys.* **15** 3535
Kochem K-H, Sohn W, Hebel N, Jung K and Ehrhardt H 1985b *J. Phys. B: At. Mol. Phys.* **18** 4455
Kochem K-H, Sohn W, Jung K, Ehrhardt H and Chang E S 1985a *J. Phys. B: At. Mol. Phys.* **18** 1253
Landolt-Börnstein 1951 *Zahlenwerte und Funktionen* vol 1 (Berlin: Springer)
Lynch M G, Dill D, Siegel J and Dehmer J L 1979 *J. Chem. Phys.* **71** 4249
Murphy W F, Holzer W and Bernstein H J 1969 *Appl. Spectrosc.* **23** 211
Nesbet R K 1979 *Phys. Rev.* A **20** 58
Rohr K 1977 *J. Phys. B: At. Mol. Phys.* **10** 2215
Sohn W, Jung K and Ehrhardt H 1983 *J. Phys. B: At. Mol. Phys.* **16** 891
Sohn W, Kochem K-H, Jung K, Ehrhardt H and Chang E S 1985 *J. Phys. B: At. Mol. Phys.* **18** 2049
Stogryn D E and Stogryn A P 1966 *Mol. Phys.* **11** 371
Szmytkowski C *13th Int. Conf. on the Physics of Electronic and Atomic Collisions, Berlin* ed J Eichler, W Fritsch, V Hertel, N Stolterhoft and U Wille (Amsterdam: North-Holland) p 242
—— 1985 Private communication
Tronc M and Azria R 1979 *Symp. on Electron-Molecule-Collisions, Tokyo* ed I Shimamura and M Matsuzawa (Tokyo: University of Tokyo Press) Invited Papers 105
Ziesel J P, Nenner I and Schulz G J 1975 *J. Chem. Phys.* **63** 1943